JAERI-M
83-219

NEUTRON YIELD MONITORS FOR THE FUSION NEUTRONICS SOURCE (FNS)

— FOR 80° BEAM LINE —

December 1983

Hiroshi MAEKAWA, Yujiro IKEDA, Yukio OYAMA
Seiya YAMAGUCHI and Tomoo NAKAMURA

日本原子力研究所
Japan Atomic Energy Research Institute

JAERI-M レポートは，日本原子力研究所が不定期に公刊している研究報告書です。
入手の問合わせは，日本原子力研究所技術情報部情報資料課（〒319－11 茨城県那珂郡東海村）あて，お申しこしください。なお，このほかに財団法人原子力弘済会資料センター（〒319-11 茨城県那珂郡東海村日本原子力研究所内）で複写による実費頒布をおこなっております。

JAERI-M reports are issued irregularly.
Inquiries about availability of the reports should be addressed to Information Section, Division of Technical Information, Japan Atomic Energy Research Institute, Tokai-mura, Naka-gun, Ibaraki-ken 319-11, Japan.

編集兼発行　日本原子力研究所
印　　刷　山田軽印刷所

JAERI-M 83-219

Neutron Yield Monitors for the Fusion Neutronics Source (FNS)
— for 80° Beam Line —

Hiroshi MAEKAWA, Yujiro IKEDA, Yukio OYAMA, Seiya YAMAGUCHI and Tomoo NAKAMURA

Department of Reactor Engineering,
Tokai Research Establishment, JAERI

(Received November 16, 1983)

A powerful D-T neutron source named FNS (Fusion Neutronics Source) has been constructed in Japan Atomic Energy Research Institute. Measurement of absolute neutron yield is essential for fusion neutronics study. The associated α-particle method is the most suitable method for the determination of absolute yield of neutrons produced by $^{3}T(d,n)^{4}He$ reaction. For the 80° beam line of the FNS, an α-monitor using a silicon surface-barrier detector (SSD) has been installed as the main neutron yield monitor. A long counter and a ^{232}Th fission counter are adopted as the sub-monitors. A thin aluminum foil is set in front of the SSD to reduce the intensity of back-scattered deuterons. The peaks in the pulse height spectrum detected by the SSD are separated by the aluminum foil and by adjusting the bias voltage of the SSD. The peaks are assigned by means of the time-of-flight method for the associated charged-particles. A method to eliminate the contribution of d-^{3}He and d-D reactions has been developed. The absolute d-T neutron yield can be estimated accurately to within less than 2 % in the best case condition. The ratios of counts of the sub-monitors to the α-monitor have been observed to be stable within their statistical errors during the same experimental period.

Keywords:

FNS, Fusion Neutronics, $^{3}T(d,n)^{4}He$, Associated α-particle Method, Absolute Neutron Yield, Long Counter, ^{232}Th Fission Counter, Silicon Surface-barrier Detector, $^{3}He(d,p)^{4}He$, $^{2}D(d,p)^{3}T$, Tritium Metal Target

核融合炉物理用中性子源(FNS)の中性子発生量モニタ
——80°ビームライン用——

日本原子力研究所東海研究所原子炉工学部
前川　洋・池田裕二郎・大山幸夫
山口誠哉・中村知夫

(1983年11月16日受理)

強力なd－T中性子源であるFNS（核融合炉物理用中性子源）が日本原子力研究所に設置された。核融合炉ニュートロニクスの研究において，絶対中性子発生量の測定は本質的な事項である。$^{3}T(d,n)^{4}He$反応で生成する中性子の絶対発生量を決定する手段として，随伴α粒子法が最も適当である。FNSの80°ビームラインにシリコン半導体検出器(SSD)を用いたαモニタを主モニタとして取付けた。また，ロングカウンタおよび^{232}Th核分裂計数管を補助モニタとして設置した。大量の後方散乱量陽子を低減するため，うすいAl箔をSSDの前に置いた。SSDで検出された波高分布の各ピークをこのAl箔とバイアス電圧を調整することにより分離した。各ピークは随伴荷電粒子に対する飛行時間法により同定した。d－^{3}Heとd－D反応の寄与を取除く方法を開発した。最良の条件において，d－T中性子の絶対発生量を2％以下の精度で算定できた。同じ実験期間中では，補助モニタとαモニタとの計数の比は統計誤差の範囲で安定であった。

Contents

目　　次

1. Introduction

In order to investigate fusion neutronics, a powerful d-T neutron source named FNS (Fusion Neutronics Source) has been constructed in Japan Atomic Energy Research Institute. The FNS consists basically of a high current electrostatic deuteron accelerator, tritium metal target assemblies, tritium handling and processing devices and experimental equipment.

The accelerator of 400 keV Cockcroft-Walton type has two ion sources —— for high and low current ——, pre- and post-acceleration pulsing devices and two drift tubes in the direction of 0° and 80° to the axis of acceleration. Each beam transport line leads to separate target rooms surrounded by a thick concrete shield: a large 15 m × 15 m target room #1 for the 80° beam line and a small 5 m × 5 m target room #2 for the 0° one. Four types of tritium metal target assemblies have been prepared: LLL-type rotating, small-sized rotating, water-cooled fixed and air-cooled fixed targets.

A variety of source conditions for experiments can be realized by suitable choices of ion sources, beam lines, operation modes —— continuous and pulse —— and target types, high intensity continuous source of initial yield up to 5×10^{12} n/sec for a sample irradiation in target room #2 or 2 ns neutron pulse with peak intensity of 10^{13} n/sec for time-of-flight experiment in target room #1 for example.

In March 1981, the FNS was completed successfully achieving the designed specifications.[1][2] The layout of the FNS accelerator system with two beam lines is shown in Fig. 1.1.

In fusion neutronics, to provide benchmark data for checking nuclear data and methods, it is very important to obtain the experimental data —— reaction rates, neutron spectra and so on —— in absolute values.[3] For this purpose, absolute measurement of neutron yield is essential for the fusion neutronics study. The associated α-particle method is only one solution to determine directly absolute yield of neutrons produced by $^{3}T(d,n)^{4}He$ reaction. It was adopted from previous experiments using the PNS-A.[3][4]

For the 80° beam line of the FNS, an α-monitor using a silicon surface-barrier detector (SSD) for associated charged-particle detection has been installed as the main neutron yield monitor. A long counter and a ^{232}Th fission counter are also adopted as the

sub-monitors. The long counter has high efficiency and flat response over a wide energy range, while the Th-fission counter has fairly low efficiency and can not detect neutrons below its threshold energy (about 1.5 MeV). As the ratios of counts of the sub-monitors to the main-monitor are stable during the same experimental period, the sub-monitors can back up the main monitor even if the main-monitor fails.

Following points are to be taken into consideration in order to achieve good accuracy with the associated α-particle method:

(1) Elimination of Rutherford scattered (back-scattered) deuterons.

The number of back-scattered deuterons detected by an α-monitor is $10^{3\sim4}$ times higher than that of α-particles. The reduction of their intensity is essential to avoid radiation damage and to observe the true α-particle count.

(2) Separation of the true α-particles of $^{3}T(d,n)^{4}He$ reaction from the α-particles of $^{3}He(d,n)^{4}He$, and from the protons of $^{3}He(d,n)^{4}He$ and of $^{2}D(d,n)^{3}T$ reactions.

Helium-3 accumulates in a target by the decay of tritium atoms, while the d-D reaction increases with the integrated product of beam current and bombardment time (mA·h).

A thin aluminum foil is set in front of the SSD to solve the problem (1), so that the effect of the back-scattered deuterons can be nearly eliminated. In order to solve problem (2), the peaks in the pulse height spectrum are separated by the use of the foil mentioned above and by adjusting the bias voltage of the SSD to optimize its depletion layer depth. The peaks are assigned by means of the time-of-flight method (TOF) for the associated charged-particles.

An outline of the monitors and their electronics are presented in Sections 2 and 3 respectively. The method of reduction of the absolute neutron yield data and error analysis are discussed in Section 4.

2. Set-up of Monitors

There are three neutron yield monitors in the first target room at FNS. They are an α-monitor, a long counter and a ^{232}Th fission counter. For the cases described in this section, the count rates of the long counter and the Th fission counter are about 8.4 times and about 0.06 times that of the α-monitor, respectively.

2.1 α-Monitor

The configuration of the 80° beam line near the target is shown in Fig. 2.1. The α-monitor is set inside the beam drift tube. A small silicon surface-barrier detector (SSD) —— Ortec BA-25-007-100 —— is used to detect the associated particles related to $^{3}T(d,n)^{4}He$ reaction. The SSD is mounted on the top of the support which is capable of height adjustment. The flange with the SSD support is mounted on a manifold illustrated in Figs. 2.1 ∿ 2.4. A 1 mmϕ aperture and a laminated aluminum foil are put in front of the SSD. The thickness of the foil is 0.41 mg/cm^2 and is enough to eliminate the most part of Rutherford scattered deuterons. Fortunately, this thickness makes it easy to separate the α-particles from the protons, i.e., when the bias voltage of the SSD is at the appropriate value, the peak of α-particle can be set between the proton peaks of $^{3}He(d,p)^{4}He$ and $^{2}D(d,p)^{3}T$. (See Fig. 4.1) The typical bias is 20 V and makes the depletion layer depth to be about 60 μm.

The manifold is fixed to keep the geometrical arrangement between the SSD and tritium targets. When a target assembly is replaced by another one, a small difference in target position may occur in which case the target may be adjusted to maintain the SSD-to-target distance constant. The adjustment is made possible by a vacuum bellows.

The distance from the target center to the aperture is 157.8 cm. The directions of incident deuteron beam and detected α-particles forms an angle of 179.1°. A sketch of this configuration is shown in Fig. 4.5.

In order to protect the SSD from the direct deuteron beam, a water-cooled aperture is placed before the manifold.

2.2 Long Counter

The long counter is placed under the grated floor, i.e., on the floor of basement near the south wall. The layout is shown in Fig. 2.5 and the photograph of the long counter is shown in Fig. 2.6. The distance from the target to the face of the long counter is 5.48 m.

The size of long counter is 40.5 cm in diameter and 52 cm in length. The design of this long counter is about the same as the standard long counter. As a BF_3 counter to be set in the long counter system, Fuji Electric Type 52152 is used. The size of this counter is 2.5 cm in diameter and 26.6 cm in active length. The pressure of $^{10}BF_3$ gas is 15 cm Hg. In the case of low neutron yield, the long counter is useful because of high efficiency.

2.3 ^{232}Th Fission Counter

The ^{232}Th fission counter is set at the support for the target assembly at the distance of 1.215 m from the target. The layout is shown in Fig. 2.7 and 2.8. The fission counter is Westinghouse Type WL-6376A and its size is 5.08 cm in diameter, 29.21 cm in length and 15.24 cm in sensitive length. The coating area and thickness of $^{232}ThO_2$ are 1070 cm^2 and 0.5 mg/cm^2, respectively.

3. Electronics for the Monitors

It is very important to use a monitor having a large dynamic range because the neutron yield of 80° beam line can vary from less than 10^7 n/s to 5×10^{11} n/s. By adopting the high current ion source (GIC 740A) and a rotating target in the future, the neutron yield is expected to be 10^{12} n/s and another α-monitor will be used. Therefore, it is desirable to use the electronics for the α-monitor that can process the pulses as fast as practical.

The block-diagram of the neutron yield monitor is shown in Fig. 3.1. In order to achieve high counting rate and to reduce the dead-time correction, a charge sensitive preamplifier —— JAERI Model 121A —— has been modified a little for the α-monitor (SSD). As the feedback resistor of 1000 MΩ has been replaced by that of 100 kΩ, the fall time of output pulse has changed from 50 μs to 400 ns. The output of the preamplifier is fed to two fast amplifiers —— Ortec 474 —— at the control room. One of them is used for the pulse counting system, while another one is used only to observe the pulse height spectrum. The differential and integral time constants of the fast amplifiers are 50 ns and 500 ns, respectively. The typical output pulse of the fast amplifier is shown in Fig. 3.2. A fast single channel analyzer (SCA) —— NAIG E-521 Universal Single Channel Analyzer —— is adopted because of its capability for short pulse width processing.

It is necessary to feed the output pulse from the SCA to a scaler, a rate meter, a CAMAC system used for data logging and so on. If the output pulse of SCA splits directly to supply these equipment, interference often occurs between them. Therefore, a logic pulse fanout —— JAERI Model 4332 —— has been developed to avoid such interference. This module has two identical circuits. Each circuit can convert a NIM fast/slow pulse to two fast and two slow pulses.

To measure the dead times of the neutron monitors, output pulses of the SCAs were observed by an oscilloscope. The output pulses of the SCA for the α-monitor are shown in Fig. 3.3. The dead times were estimated to be about 0.3 μs and about 1.5 μs for the α-monitor and the long counter respectively, from the time interval to the next closest pulse. The dead time of Th-fission counter was not measured because of its low count rate.

4. Absolute Neutron Yield Determination from the α-Monitor

4.1 Identification of Charged Particles in Pulse Height Spectrum

To estimate the yield of neutrons produced by $^{3}T(d,n)^{4}He$ reaction, it is necessary to detect only the associated α-particles by the SSD. Unwanted particles are usually produced at the same time by parasitic reactions, i.e., $^{3}He(d,p)^{4}He$, $^{2}D(d,n)^{3}He$ and $^{2}D(d,p)^{3}T$. Helium-3 in the target is accumulated by the decay of tritium, while deuterium is implanted on the target by an accelerated deuteron beam.

A typical pulse height spectrum of the SSD is shown in Fig. 4.1. As the detector bias is adjusted to separate the pulse height peaks of particles by the difference of energy deposit in the depletion layer, there are two peaks in the spectrum besides the large peak corresponding to the α-particle of d-T reaction. The α-particle produced by d-^{3}He reaction has almost the same energy as that by d-T reaction. Thus the α-particle by d-^{3}He interferes with the main peak. The pulse height spectrum has a tail to the lower energy side of peaks due to straggling in the foil.

In order to identify the peaks in the spectrum, the pulse height spectrum of SSD was analyzed by means of the time-of-flight method using the intense pulse beam of FNS. Associated particle reactions, their energy and flight time are summarized in Table 4.1. Typical pulse height and arrival time spectra are shown in Figs. 4.2 and 4.3, respectively. As is evident from the Table 4.1 and Fig. 4.3, both α-particles produced by d-T and d-^{3}He reactions were not separated in the time spectrum because their arrival time were almost the same. Protons produced by d-D and d-^{3}He reactions were clearly isolated from the α-particles. The pulse height spectrum was measured by gating a multichannel analyzer corresponding to the interval time for each particle. The correspondence of pulse height spectrum for each time region is shown in Fig. 4.4.

It became clear from Fig. 4.4 that the large peak in the pulse height spectrum was corresponding to the α-particles of d-T and d-^{3}He reactions. As the target used in this TOF experiment was about 2 years old from its production, the accumulation of Helium-3 was clearly observed as the lower peak in the pulse height spectrum. But the rate of d-D reaction was small in this case, because the target was not

used for extensive beam exposures and the implantation of deuterium in the target was very little. It was difficult to distinguish the proton by d-D reaction by the TOF method, however, the higher peak in the spectrum was obviously corresponding to the proton by $^{2}D(d,p)^{3}T$ reaction through the energy spectrum measurement. For example, this peak can be seen in Fig. 4.1. It has been observed in our experiments that the peak increased gradually with the usage of a target. This fact supports the above result. The proton energy of d-^{3}He is higher than that of d-D reaction, however, the energy deposit in the SSD is smaller because of its high energy and rather thin depletion layer of the SSD.

There exists the component at the lower side in the pulse height spectrum. This component decreases almost exponentially with the pulse height. As this component was observed in the three gated pulse height spectra in Fig. 4.4, it is caused by the back-scattered deuterons.

In this investigation, we can identify each peak in the spectrum. Thus the contamination in the α-peak is only by d-^{3}He reaction which can be estimated by its associated proton peak.

4.2 Estimation of Absolute Neutron Yield

The absolute total neutron yield at the target Y_n is given by the relation;

$$Y_n = \frac{4\pi}{\Delta\Omega} \cdot C_\alpha \cdot R_\alpha (E_d, \theta_\alpha) \quad , \tag{1}$$

where $\Delta\Omega$ is the solid angle of the target subtended by the detector aperture, C_α the true count of α-particles detected by the SSD and R_α the anisotropy correction factor whose value depends on the incident energy E_d and the emitted angle of α-particle θ_α.

The solid angle $\Delta\Omega$ is given by;

$$\Delta\Omega = \frac{(b/2)^2 \cos\theta_\alpha}{L^2 + r^2} \quad [sr] \quad , \tag{2}$$

The parameters in Eq. (2) are shown in Fig. 4.5 and these values are as follows:

L = (1578 ± 1) mm, r = (25 ± 1) mm, b = (0.9835 ± 0.0054) mm and θ_α = 179.1°. Then the solid angle $\Delta\Omega$ is,

$$\Delta\Omega = (3.050 \pm 0.034) \times 10^{-7} \quad .$$

The determination of C_α is described in the following Section. The calculation of R_α and its error is discussed is Ref. (5) in detail. The factor R_α used at FNS is shown in Table 4.2.

4.3 Determination of the True α-Count

The determination of true α-count C_α is usually not so easy to keep its precision maximum, especially in the case of a high current beam operation, because the SSD is affected gradually by radiation damage. We have developed the following two methods from which we may choose depending on the experimental situation and demand.

(A) Precise estimation method

The pulse height spectrum should be observed for the whole time during each experimental run. The following conditions must be satisfied:

i) the count-rate is not high enough to cause excessive pulse pileup,

ii) overflow never occurs at any channel during the experimental run.

The procedure is explained in an orderly manner using Fig. 4.1 as a sample spectrum. The MCA used in the experiment must be adjusted so that its zero channel corresponds to the zero pulse height. The calculations in the following steps can be done using the standard functions of a commercial MCA.

Step A-1

After the acquisition of the spectrum, upper and lower channels —— namded N_L and N_U —— are set between peaks A and B, and between peaks B and C, respectively, where peaks A, B and C correspond to the protons of d-^{3}He, the α-particles of d-^{3}T and d-^{3}He and the protons of d-D reactions, respectively. In this typical case, they are given by:

$$N_L = 0.705\ N_p, \quad N_U = 1.625\ N_p \quad ,$$

where N_D is the peak channel of peak B. As the factors, 0.705 and 1.625, depend on the condition of a SSD, it is necessary to find them for each observed spectrum. Then, integral count C_B between N_L and N_U can be obtained.

Step A-2

Select the nearly flat region including the channel N_L, i.e., the channels having almost the same count-rate. This region has usually more than 30 channels. Calculate the average count of this region $\bar{C}_L$.

Step A-3

Calculate the total area count C_A by use of the function of the MCA.

Step A-4

We can obtain the true count for the reaction $^3T(d,n)^4He$ detected by the SSD. The count is given by

$$C_\alpha = C_B + \bar{C}_L(N_L - 1) - K \cdot C_A \ , \tag{3}$$

where K is the conversion factor from the proton count by d-^{3}He reaction detected by the SSD to the contribution of α-count by d-^{3}He reaction in the peak B. The factor K shown in Table 4.2 is dependent on the incident deuteron energy E_d and angle θ_α.

(B) Alternate method

This method seems to be practical because the accuracy is fairly good and the procedure is easy compared to method (A).

The factor F is defined as;

$$F = 1 + \frac{\bar{C}_L \cdot (N_L - 1) - K \cdot C_A}{C_B} \tag{4}$$

Then Eq. (3) can be written;

$$C_\alpha = F \cdot C_B \ . \tag{5}$$

If the α-monitor system is stable during the experiment, the factor F is assumed to be constant. When the factor F is determined by using the typical observed spectrum, C_α can be estimated from the total count C_B during each experimental run. If a peak shift occurs during the experiment and is not large, the changes of total count C_B and factor F compared to the real ones are very small, because the contribution around the channels N_L and N_U is small. Though the effect of peak shift due to SSD damage or the drift of electronics is small, it is advisable to measure the spectrum periodically during the experiment and to check its shape and factor F.

Step B-1

Set the lower and upper levels of the fast SCA corresponding to N_L and N_U.

Step B-2

Determine the factor F for a typical pulse height spectrum using Eq. (4).

Step B-3

Measure the total count C_B by a scaler during each experimental run.

Step B-4

We can obtain the total α-count detected by the SSD using Eq. (5).

4.4 Error Analysis for the α-Monitor

The systematic error in a observed absolute neutron yield is divided into the following three factors. The statistical (random) error in the total count C_B is usually small enough to neglect.

(1) The error in the solid angle

This error is evaluated to be 1.10 % in the previous section and mainly caused by the uncertainty of the aperture size.

(2) The error in the conversion factor R_α

According to the examination described in Ref. (5), the tritium distribution in a titanium layer of the target affects the calculated result of R_α. In this calculation, a model for the tritium profile shown in Fig. 4.6 was adopted according to the experiments.(6) The R_α does not change very much with the parameters a and b but with the parameter E_a. In the case that E_d = 400 keV, the difference of R_α is about 3 % between an ideal model (a = b = 1, $E_a = E_d$ = 400 keV) —— a flat distribution —— and a completely used target model (a = 0.6, b = 0.4, E_a = 35 keV). The actual tritium profile in a target can not be measured on-line and varies from the initial state to the final state. Therefore we must assume the profile to determine the factor R_α and have decided on the parameters 0.8, 0.6 and $\frac{1}{2} E_d$ for a, b and E_a, respectively. The actual value of conversion factor R_α might be between those of ideal and ending profiles, however, the error of R_α using the assumed profile is within about ± 1.5 %. The factor R_α and its expected maximum error are tabulated in Table 4.2.

(3) The error in the true count C_α

The assigned error in the C_α depends on its method of estimation. The determination of this error is necessary to consider the condition of α-monitor during each experimental run. Typical evaluation for the two cases cited in 4.3 is shown as follows:

(A) Precise estimation method

In this case, a total count C_α is obtained by using an observed spectrum during the entire time of each experimental run. The main factors of error in C_α are classified into four.

i) The error in the correction of d-^{3}He reaction

The atom number of ^{3}He in a target depends on its history. In the case of a very fresh target, the d-^{3}He reaction is negligible naturally, while the ratio C_A/C_B is a few percent for a fairly old target. Therefore the error due to the correction of d-^{3}He reaction can be neglected.

ii) The error in the extrapolation to zero pulse height

The integral linearity of a MCA is less than 0.1 % and it is easy to adjust the zero pulse height to within ± 1 channel. Even if the actual channel corresponding to the zero pulse height is ± 5 channel, the error is only ± 0.12 % for a typical case.

iii) The error due to pulse pileup

As the pulse width of the fast amplifier is almost the same as the observed dead time (0.3 μs), it can be assumed that the probability of chance coincident pulses is in proportion to product of the dead time and count rate. This correction is estimated to be about 0.5 % for the neutron yield of 5×10^{11} n/s, and the error can be neglected adopting the following correction factor f_s;

$$f_s = 1 + 2\,n\tau \quad , \tag{6}$$

where n is the count rate and τ the dead time.

(iv) The error due to back-scattered deuterons

The pulse height distribution of back-scattered deuterons seems to decrease exponentially as a function of channel number. Assuming the distribution to be an exponential function, the contirbution to the average count $\bar{C}_L$ is negligible for a typical spectrum.

(B) Alternate method

In this method, the error in C_α can be separated into two factors:

i) The error in a count C_B

This error is caused by the peak shift due to the damage of SSD and the drift of electronics used in the α-monitor. Even if the total shift is assumed to be 20 channels, the effect is only 0.4 % for a typical case.

ii) The error in factor F

This error can be minimized by means of periodical observation of the pulse height spectrum and is equal to that of method (A) for the best condition.

The typical error of absolute neutron yield estimated by this α-monitor for the method (A) is given by the relation;

$$\left(\frac{\delta Y}{Y}\right)^2 \leqq \left(\frac{\delta(\Delta\Omega)}{\Delta\Omega}\right)^2 + \left(\frac{\delta R_\alpha}{R_\alpha}\right)^2 + \left(\frac{\delta C_\alpha}{C_\alpha}\right)^2$$

$$= 1.10^2 + 1.50^2 + 0.12^2$$

$$\therefore \quad \frac{\delta Y}{Y} \leqq 1.9\ \%$$

The error of method (B) is close to that of method (A) for a stable case. For a high current and long run experiment, it has been observed that the pulse height spectrum was changed with time. In that case, the estimated error was 3 ∿ 4 %.

5. Summary

(1) In order to estimate the absolute neutron yield, an α-monitor has been installed on the 80° beam line of FNS as the main monitor. A long counter and a ^{232}Th fission counter have also been installed to supplement the α-monitor.

(2) A method to eliminate the contribution of d-^{3}He and d-D reactions has been developed. The absolute d-T neutron yield can be estimated accurately to within less than 2 % for the best case condition.

(3) As the α-monitor is placed inside of the beam drift tube, an experimental assembly and related equipment have no effect on the α count but does on the long counter and the fission counter. The ratio of counts among the three monitors was observed to be stable within their statistical errors during the same experimental period.

(4) In this study, d-D neutrons have not been considered because the contribution of d-D neutrons is only a few percent of d-T neutrons in the worst case. Further investigation should be necessary to estimate the contribution of d-D neutrons.

Acknowledgement

The authors thank Messrs. J. Kusano, C. Kutsukake and S. Tanaka for their operation of the FNS accelerator. They are grateful to Dr. G. DiIorio for his helpful review of this manuscript.

5. Summary

(1) In order to estimate the absolute neutron yield, an α-monitor has been installed on the 80° beam line of FNS as the main monitor. A long counter and a ^{232}Th fission counter have also been installed to supplement the α-monitor.

(2) A method to eliminate the contribution of d-^{3}He and d-D reactions has been developed. The absolute d-T neutron yield can be estimated accurately to within less than 2 % for the best case condition.

(3) As the α-monitor is placed inside of the beam drift tube, an experimental assembly and related equipment have no effect on the α count but does on the long counter and the fission counter. The ratio of counts among the three monitors was observed to be stable within their statistical errors during the same experimental period.

(4) In this study, d-D neutrons have not been considered because the contribution of d-D neutrons is only a few percent of d-T neutrons in the worst case. Further investigation should be necessary to estimate the contribution of d-D neutrons.

Acknowledgement

The authors thank Messrs. J. Kusano, C. Kutsukake and S. Tanaka for their operation of the FNS accelerator. They are grateful to Dr. G. DiIorio for his helpful review of this manuscript.

References

(1) Nakamura T., et al.: "Fusion Neutronics Source (FNS)," Proc. 3rd Symp. on Accelerator Sci. & Technol., Osaka Univ., Aug. 27-29, 1980, pp. 55-56.

(2) Nakamura T., et al.: "Present Status of the Fusion Neutronics Source (FNS)," Proc. 4th Sym. on Accelerator Sci. & Technol., RIKEN Saitama, Nov. 24-26, 1982, pp. 155-156.

(3) Maekawa H., Seki Y.: J. Nucl. Sci. Technol. 14, 97 (1977)

(4) Maekawa H., et al.: ibid. 16, 377 (1979)

(5) Yamaguchi S., Oyama Y., Maekawa H.: "Calculation of Anisotropy Correction Factor for Determination of D-T Neutron Yield by Associated α-Particle Method," To be published in JAERI-M report.

(6) Davis J.C., Anderson J.D.: J. Vac. Sci. Technol., 12, 358 (1975)

Table 4.1 Associated particle reactions

Reaction type	Q value (MeV)	Particle	Energy (MeV) (θ = 179°)	Flight time (ns) (ℓ = 1.578 m)
$^{3}T(d,n)^{4}He$	17.6	n	13.32	31.8
		^{4}He	2.74	137.8
$^{3}He(d,p)^{4}He$	18.35	p	13.90	30.6
		^{4}He	2.87	134.7
$^{2}D(d,n)^{3}He$	3.27	n	2.08	79.0
		^{3}He	0.45	294.9
$^{2}D(d,p)^{3}T$	4.03	p	2.61	70.6
		^{3}T	0.59	257.0

* Incident deuteron energy is 160 keV which is mean reaction energy for the 310 keV acceleration.

Table 4.2 Anisotropy correction factor R_α, its expected maximum error and factor K for Ti-T target

E_d [keV]	R_o *1	R_α	Error [%] *2	K *3
200	1.2417	1.2239	1.45	0.8049
205	1.2435	1.2257	1.45	0.8022
210	1.2452	1.2275	1.44	0.7995
215	1.2469	1.2292	1.44	0.7968
220	1.2485	1.2310	1.42	0.7941
225	1.2501	1.2326	1.42	0.7914
230	1.2517	1.2343	1.41	0.7888
235	1.2532	1.2359	1.40	0.7862
240	1.2547	1.2374	1.40	0.7837
245	1.2562	1.2389	1.40	0.7812
250	1.2577	1.2405	1.39	0.7787
255	1.2591	1.2419	1.38	0.7762
260	1.2605	1.2433	1.38	0.7738
265	1.2618	1.2448	1.37	0.7714
270	1.2632	1.2462	1.36	0.6790
275	1.2645	1.2475	1.36	0.7667
280	1.2657	1.2488	1.35	0.7643
285	1.2670	1.2501	1.35	0.7620
290	1.2683	1.2515	1.34	0.7598
295	1.2595	1.2528	1.33	0.7575
300	1.2707	1.2539	1.34	0.7553
305	1.2719	1.2552	1.33	0.7531
310	1.2731	1.2564	1.33	0.7510
315	1.2743	1.2577	1.32	0.7489
320	1.2755	1.2588	1.33	0.7468
325	1.2767	1.2600	1.33	0.7447
330	1.2779	1.2611	1.33	0.7427
335	1.2791	1.2623	1.33	0.7407
340	1.2802	1.2634	1.33	0.7387
245	1.2814	1.2645	1.34	0.7368
350	1.2825	1.2656	1.34	0.7349
355	1.2837	1.2667	1.34	0.7331
360	1.2848	1.2678	1.34	0.7312
365	1.2860	1.2689	1.35	0.7295
370	1.2871	1.2700	1.35	0.7277
375	1.2882	1.2710	1.35	0.7260
380	1.2893	1.2720	1.36	0.7244
385	1.2904	1.2731	1.36	0.7227
390	1.2915	1.2741	1.37	0.7211
395	1.2926	1.2752	1.36	0.7196
400	1.2937	1.2761	1.38	0.7180

*1 The factor for the ideal tritium profile

*2 This error means difference between R_o and R_α. The error of R_α can be less than this value.

*3 The conversion factor from proton to α-particle counts for $^3He(d,p)^4He$ reaction.

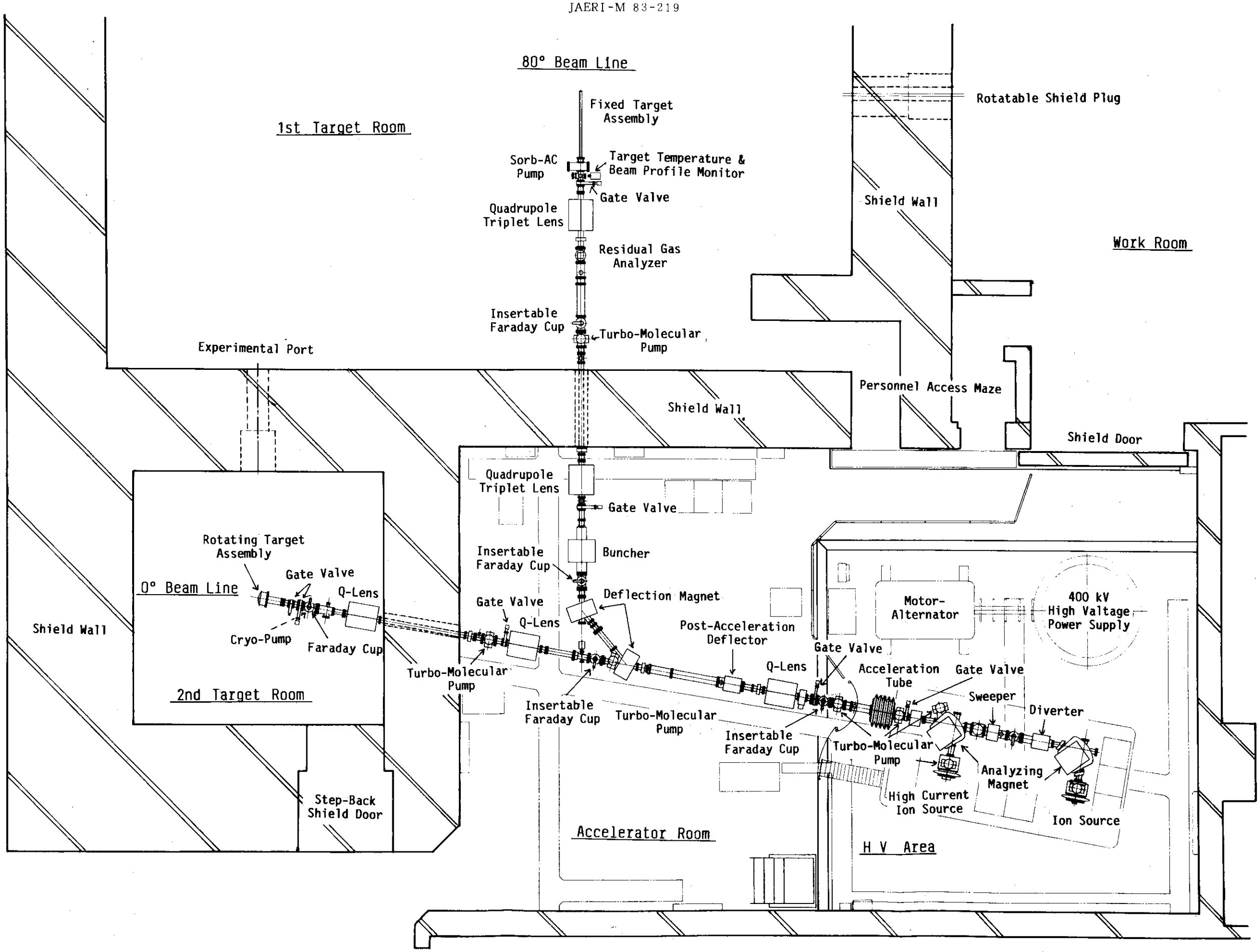

Fig. 1.1 Layout of FNS accelerator system with two beam lines

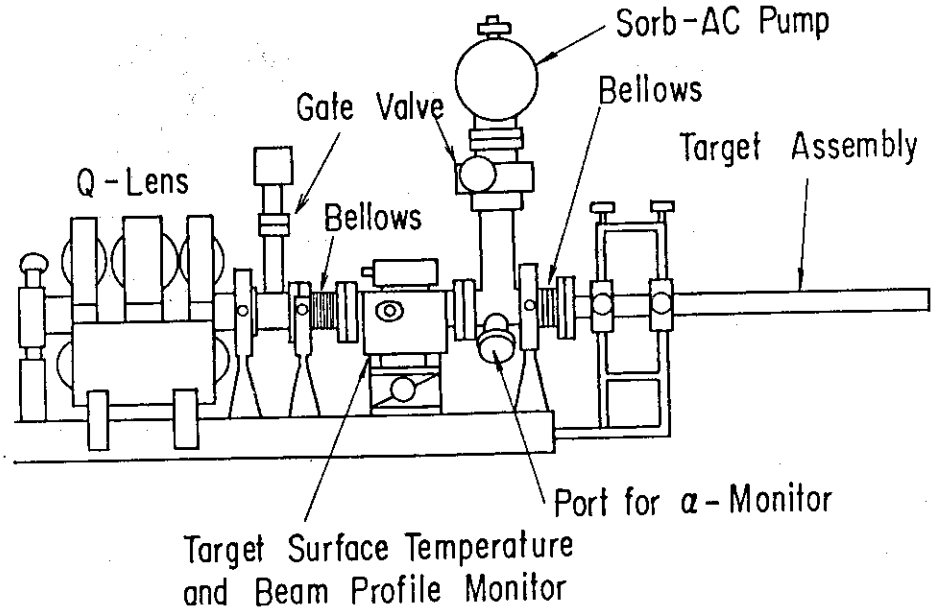

Fig. 2.1 Configuration of 80° beam line near the target

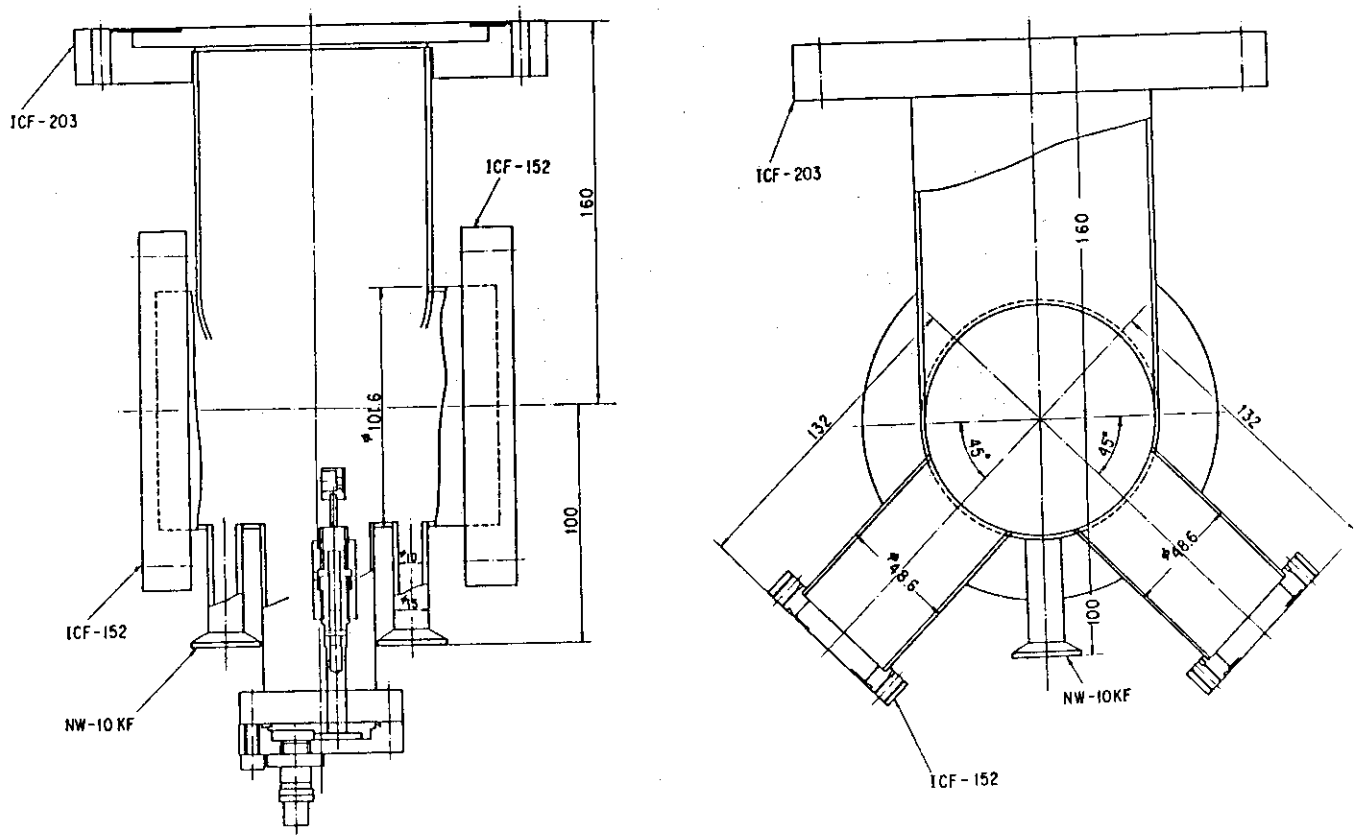

Fig. 2.2 Manifold for the α-monitor and vacuum exhaust ports

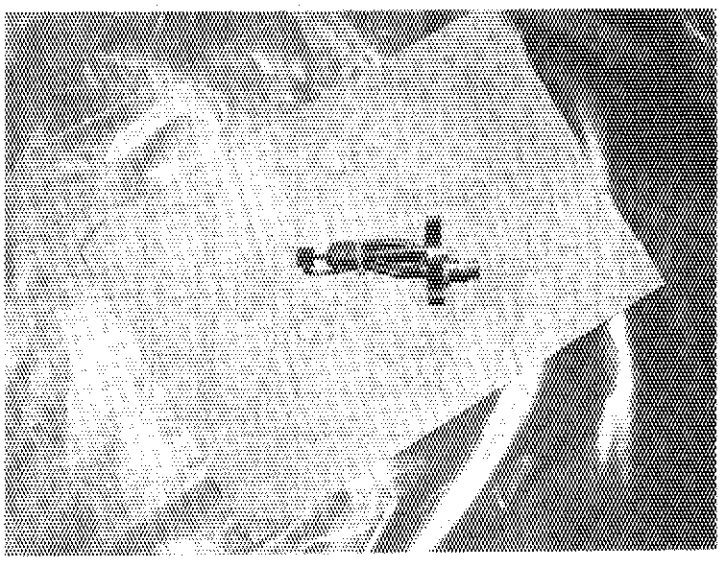

Fig. 2.3 Small silicon surface-barrier detector and its support

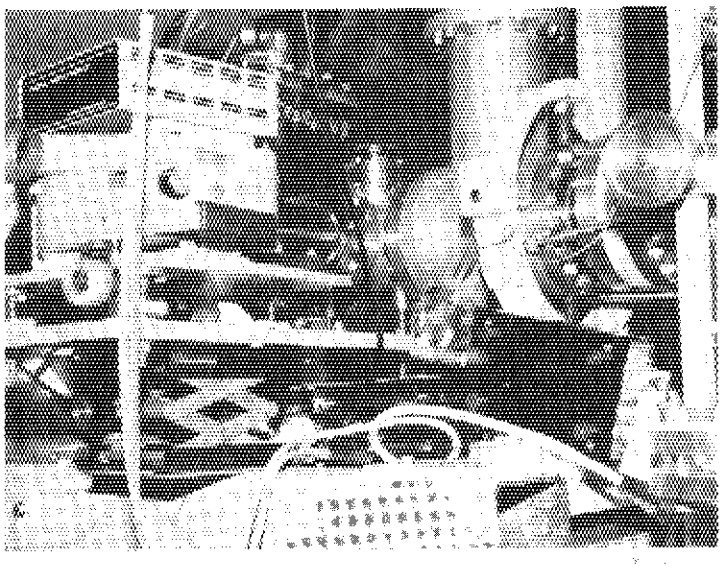

Fig. 2.4 A view of the manifold

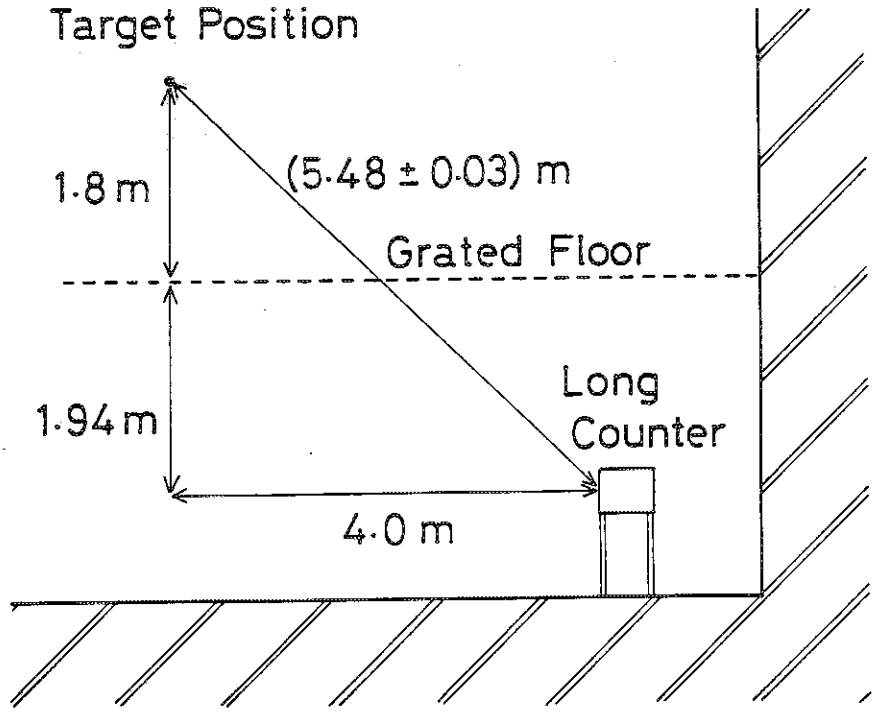

Fig. 2.5 Layout of the long counter
This figure shows the cross-section at the target position perpendicular to the beam line.

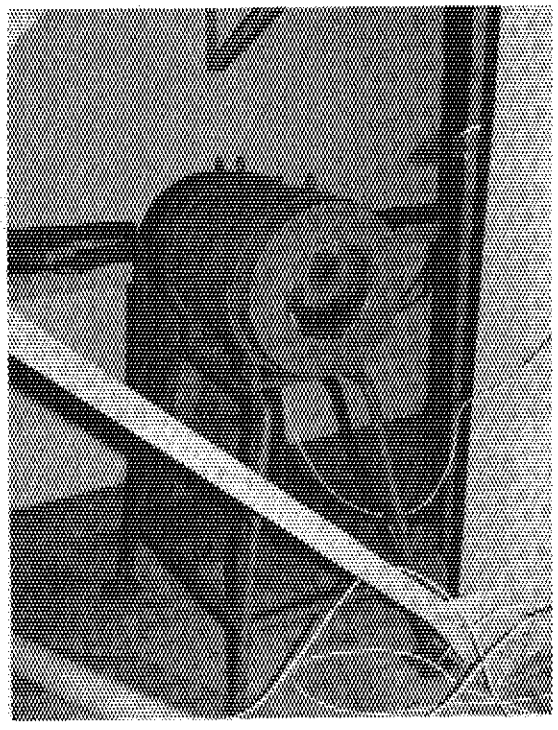

Fig. 2.6 Long counter

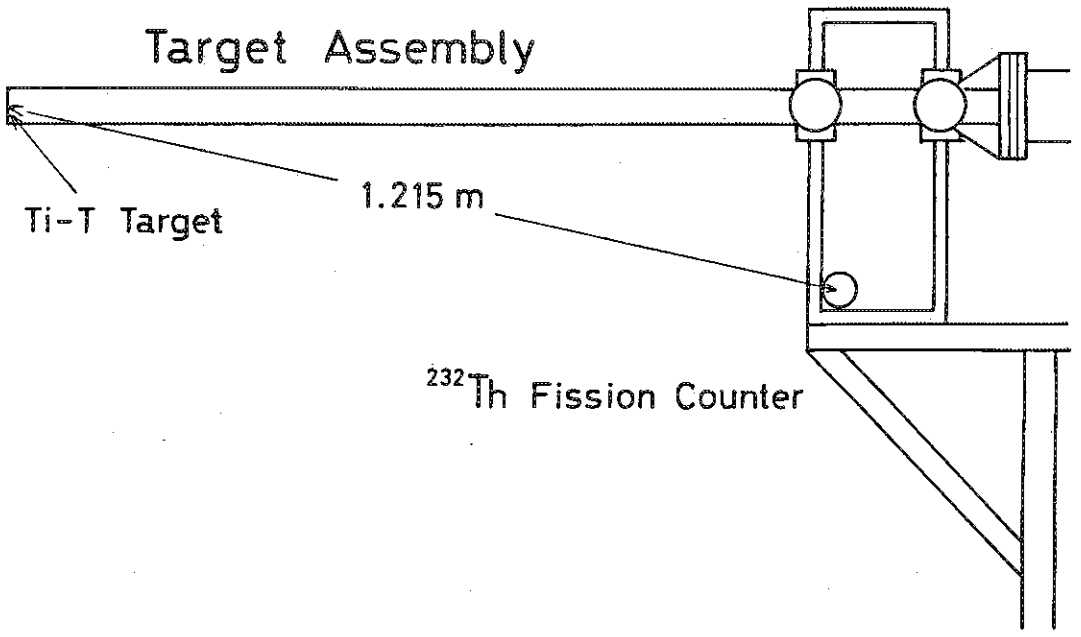

Fig. 2.7 Layout of the ^{232}Th fission counter

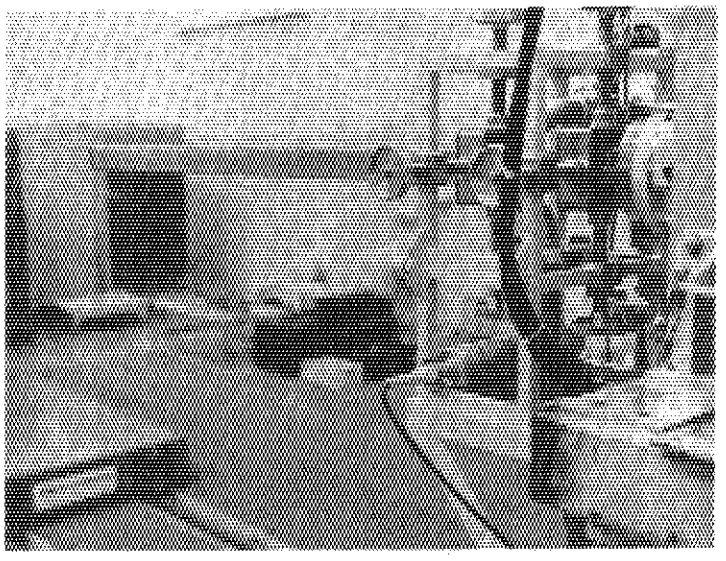

Fig. 2.8 Thorium-232 fission counter

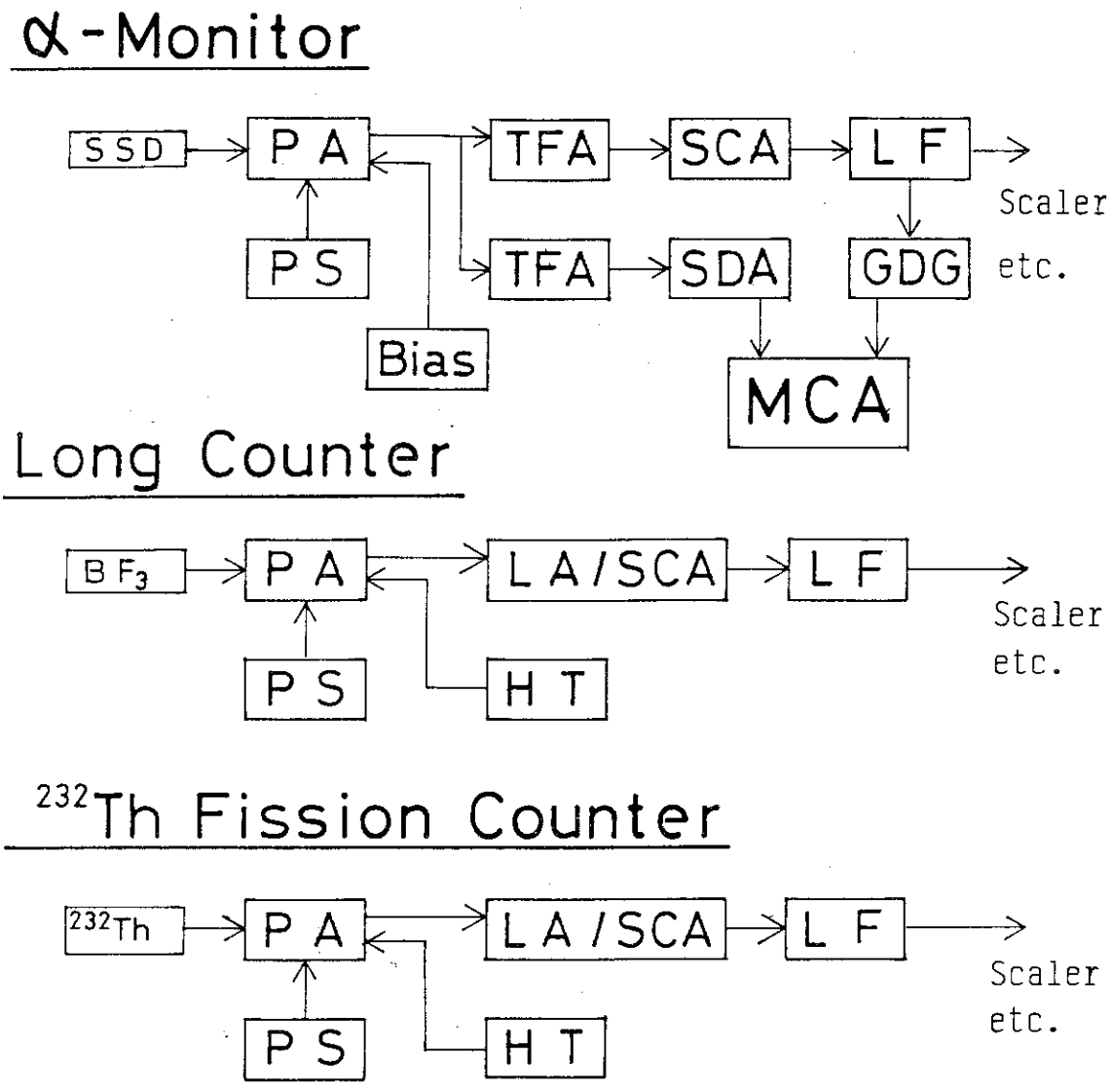

PA : Pre-Amplifier TFA : Timing Filter Amplifier

PS : Power Supply SCA : Single Channel Analyzer

LF : Logic Pulse Fanout SDA : Sum Delay Amplifier

LA : Linear Amplifier GDG : Gate and Delay Generator

HT : High Voltage Power Supply

Fig. 3.1 Block-diagram of electronics for the 80° beam line neutron yield monitors

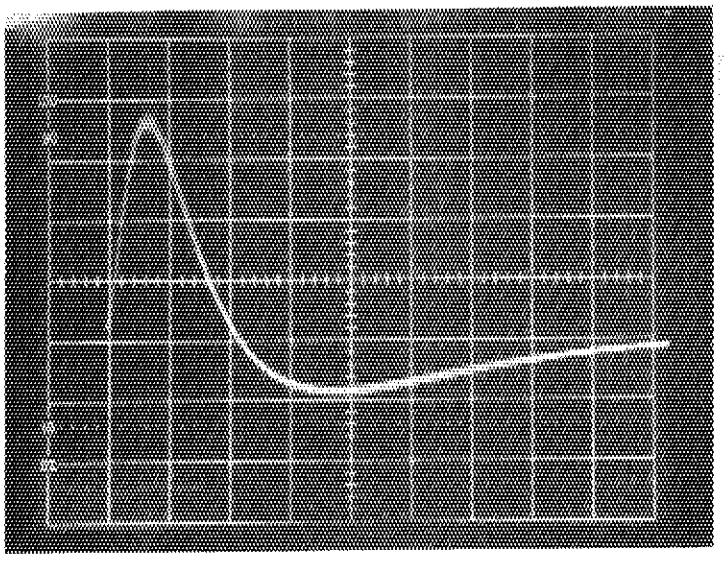

Fig. 3.2 Typical output pulse of the fast amplifier
Horizontal and vertical scales are 200 ns/div and 0.5 V/div, respectively.

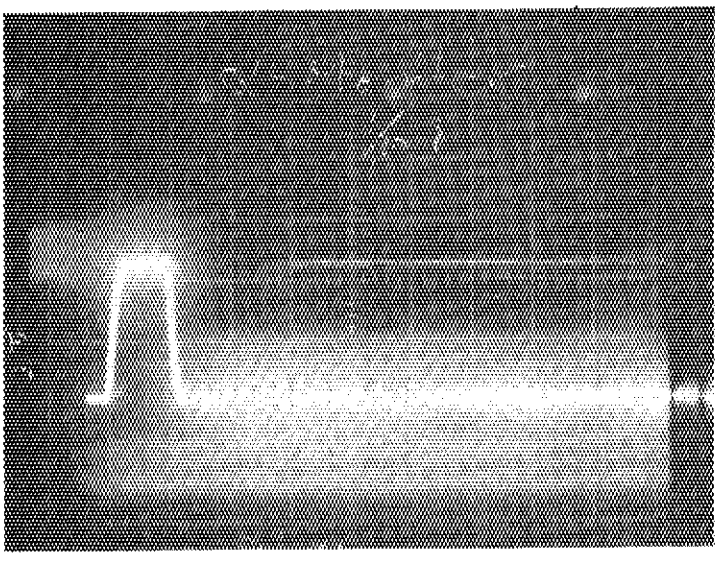

Fig. 3.3 Output pulse of the fast single channel analyzer
Horizontal and vertical scales are 0.1 μs/div and 2 V/div, respectively. It can be seen that next closest pulse is coming after about 0.3 μs.

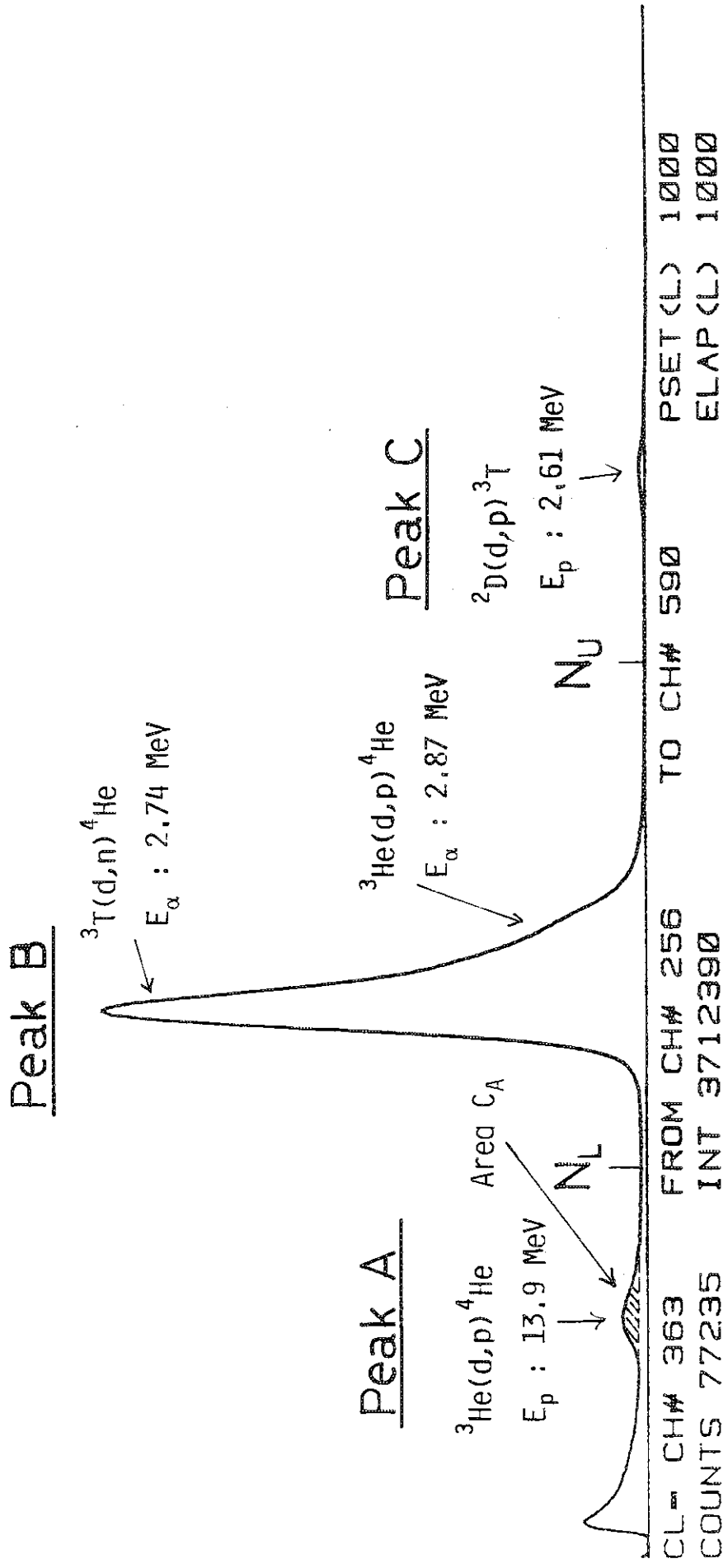

Fig. 4.1 Typical pulse height spectrum of the SSD in linear scale

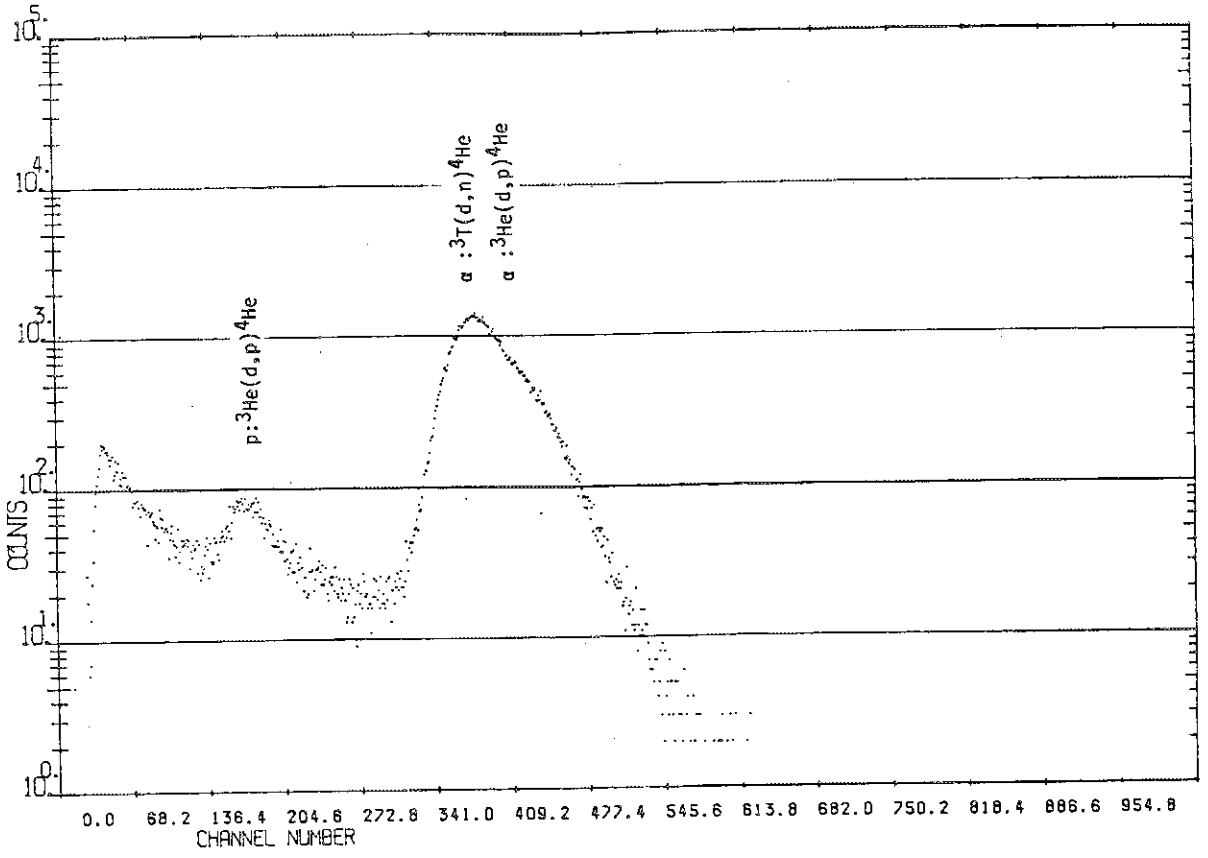

Fig. 4.2 Typical pulse height spectrum of the SSD during the TOF analysis

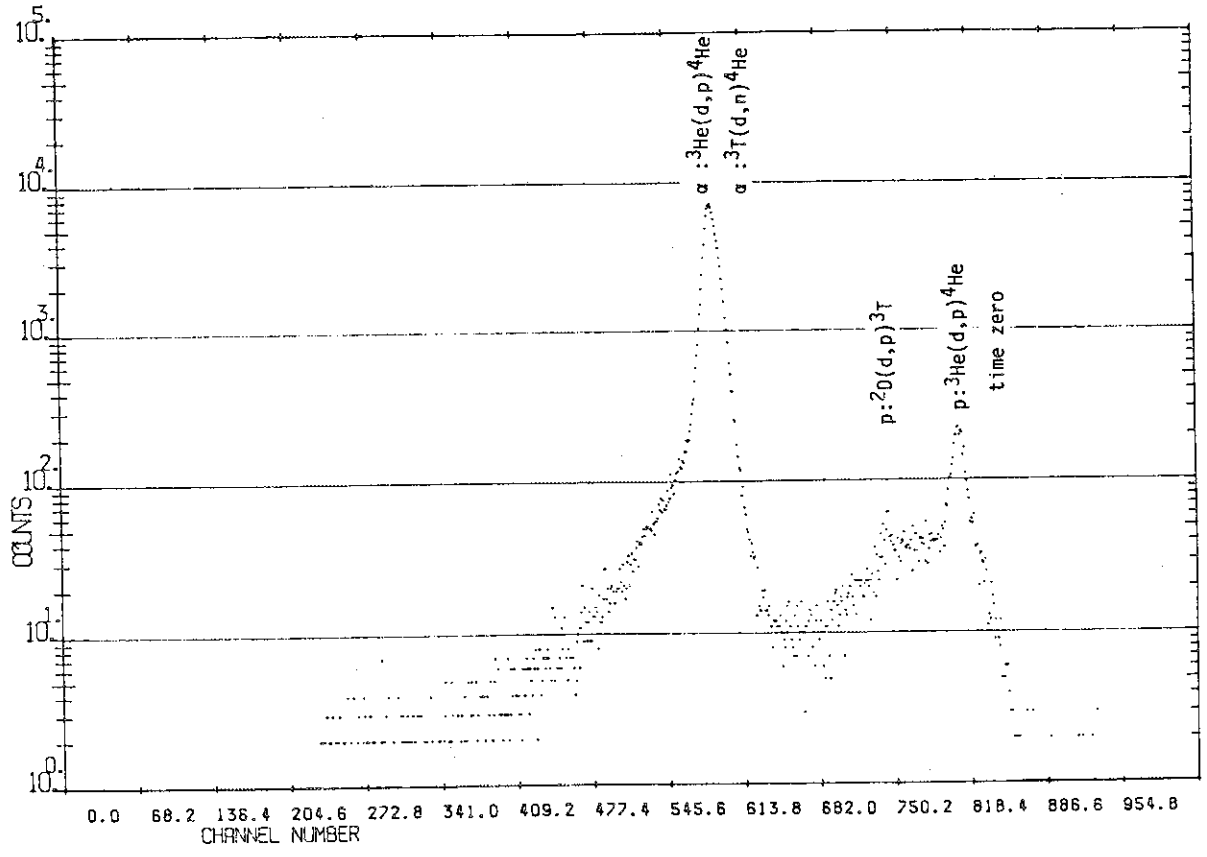

Fig. 4.3 Arrival time spectrum of associated particles

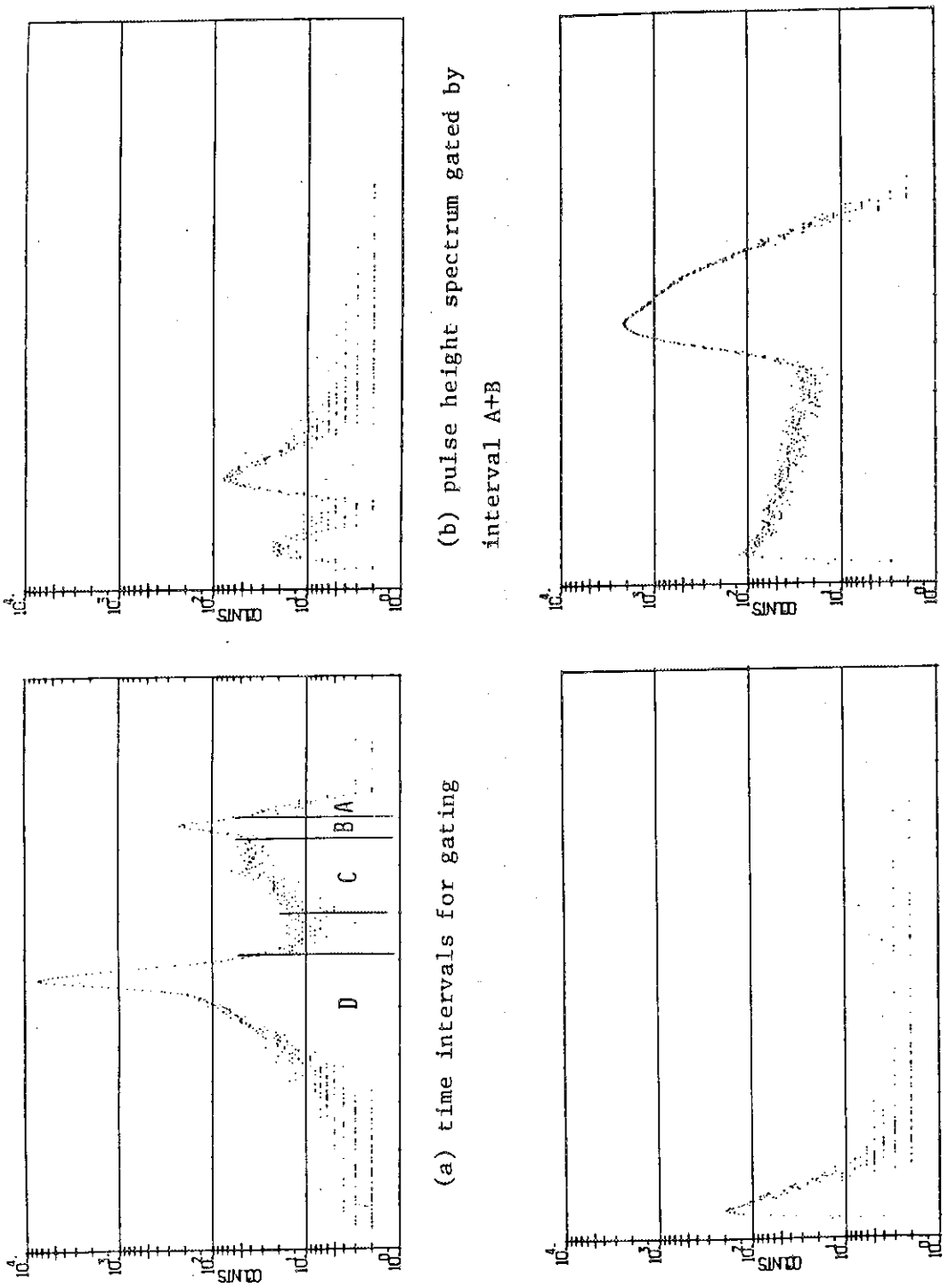

(a) time intervals for gating

(b) pulse height spectrum gated by interval A+B

(c) pulse height spectrum gated by interval C

(d) pulse height spectrum gated by interval D

Fig. 4.4 Time gated pulse height spectra for various time intervals

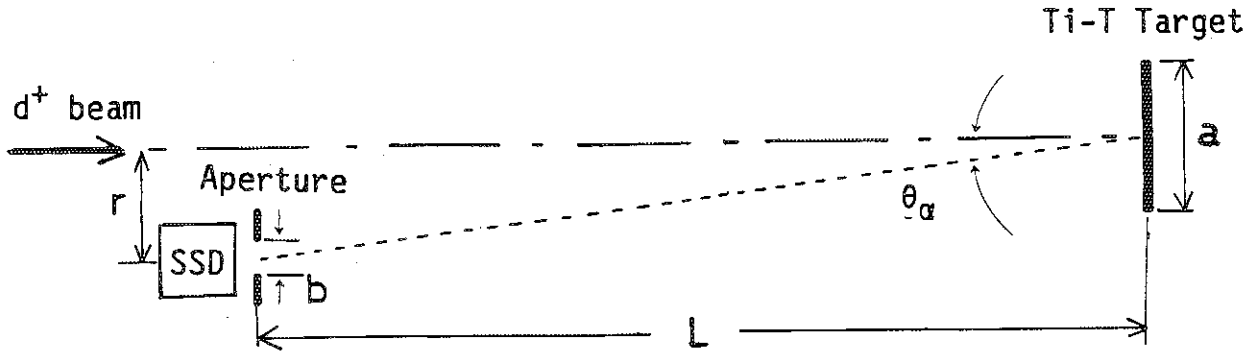

a = ~ 10 mm b = (0.9835 ± 0.0054) mm

L = (1578 ± 1) mm r = (25 ± 1) mm

θ_α = 179.1°

Fig. 4.5 A sketch of geometrical configuration of the α-moniter

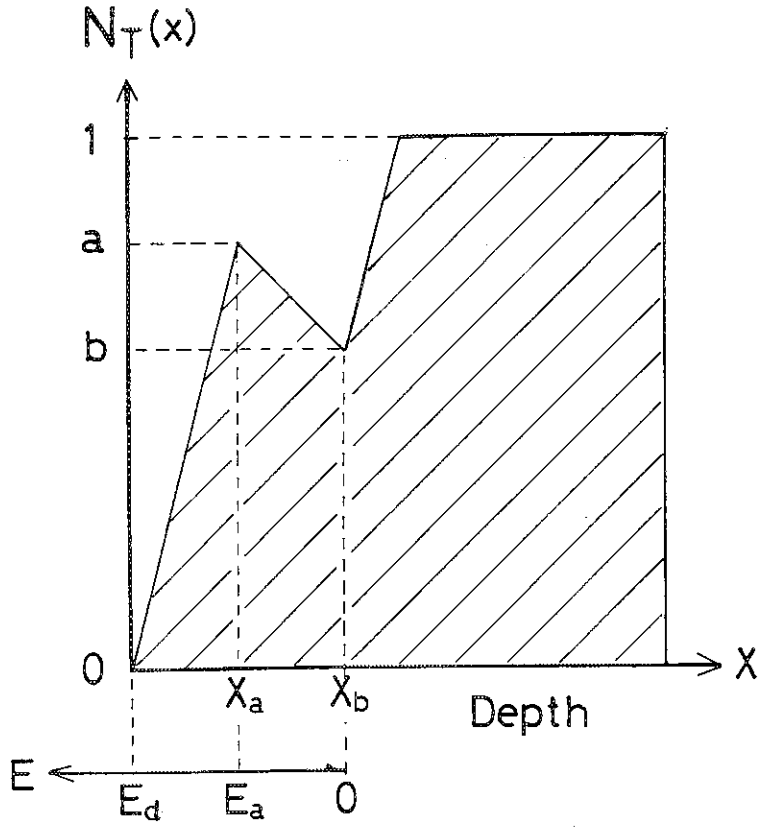

Fig. 4.6 A model of tritium depth profile based on an experiment[6]